Appl. Phys. B 68, 1061–1067 (1999) / DOI 10.1007/s003409901496

Applied Physics B
Lasers
and Optics

Recording grooves for fiber-chip coupling in PMMA using KrF excimer laser radiation: experiment and simulation

T. Sterkenburgh[1], H. Franke[1], M. Becker[2], M. Garen[2], W.F.X. Frank[3]

[1] Fachbereich Physik, Gerhard Mercator-Universität-GH Duisburg, 47048 Duisburg, Germany
[2] Fachbereich Physikalische Technik, FHO Emden, 26721 Emden, Germany
[3] FI Deutsche Telekom, 64295 Darmstadt, Germany

Received: 7 December 1998/Revised version: 12 January 1999/Published online: 12 April 1999

Abstract. The fabrication of deep grooves with a high aspect ratio in poly-methylmethacrylate using excimer laser radiation (248 nm) and a cylindric lens has been investigated. The form of the grooves and their dimensions are evaluated with respect to the recording parameters. The patterns and their widths and depths may be adapted in a wide range depending on the particular application. As an example grooves for coupling monomode optical silica fibers were fabricated.

Simulations were performed in order to explain the pattern formation. In a simple model the thermo-optic etching process may be simulated using a Gaussian-shaped laser beam and the FDBPM approach.

PACS: 81.20; 78.30; 78.20

One major advantage of using polymers for integrated- or micro-optic devices is the large variety of methods for patterning the material. Besides the standard techniques known from microelectronics such as photoresist technology (which is already a photopolymer), reactive ion etching, electron-beam or ion-beam patterning, including wet-etching methods, polymers may be patterned by light in a self-developing manner. There are two principles, the photolytic one and the thermal decompostion technique. For the photolytic way organic bonds such as C−C or C=C, C=O, C−H, etc. are decomposed by energy UV photons. In case of poly-(methylmethacrylate) (PMMA) the wavelength for the direct photolytic decomposition has to be below 300 nm [1, 2]. This can be read from the absorption spectrum of pure PMMA, which is transparent in the visible range for $\lambda \geq 300$ nm. If longer wavelength light sources have to be used, the material has to be doped and the decomposition can be obtained for high absorbed energies. Then a photothermal decomposition technique is used.

The absorption coefficient of polymers rises again in the infrared region. In the spectral range of the readily available high-power CO_2 lasers (10.6 μm) absorption coefficients up to $10^5\,\mathrm{cm}^{-1}$ are reported [3, 4] for PMMA. Therefore thick polymer samples of several mm may be cut by CO_2 laser [5] using the thermo-optic decomposition. High-power CO_2 lasers are used for cutting metals, see for example [6]. Wide waveguide patterns (≥ 200 μm) have been recorded computer-controlled using a CO_2 laser at low average power of about 1 W [7, 8].

Using KrF excimer laser radiation a high resolution of the patterns may be achieved due to the short wavelength of 248 nm. For this paper we picked an example for a 3-dimensional pattern of a set of grooves for coupling monomode fibers to a chip in a given distance. The width of the grooves is given by the diameter of the cladding in the order of 120–140 μm, the aspect ratio (depth/width) of the pattern is about 1. These grooves should be an alternative to the anisotropic wet-etching process in silicon. The accuracy of the fiber adjustment should be in the order of 1 μm in all three directions. Will we be able to copy the V-shaped grooves of the silicon etching? Can we even control the shape? To answer these questions we also made model simulations of the 3-dimensional light intensity distribution prior to the etching process to compare with the experimentally obtained patterns. The local intensity distribution will influence the etching front in the photothermal decomposition.

1 Experimental

1.1 The coupling concept

The fiber-chip coupling is one of the most important processes in introducing integrated optical devices. Our approach is demonstrated in Fig. 1. We assume an arbitrary waveguide pattern on a chip with the requirement of coupling monomode fibers to certain input channels. Let the surface area of the chip be the *yz* plane with the *z* axis parallel to the input channel. Then the *y* positions of the input channels (y_i) are determined for example from the photomask of the particular structure, whereas the *x* positions are all the same. As shown in Fig. 1 we propose a "bench" concept, where the whole set of the input array of channel to fiber coupling can

The authors would like to dedicate this paper to Prof. Dr. Eckard Krätzig on the occasion of his 60th birthday.

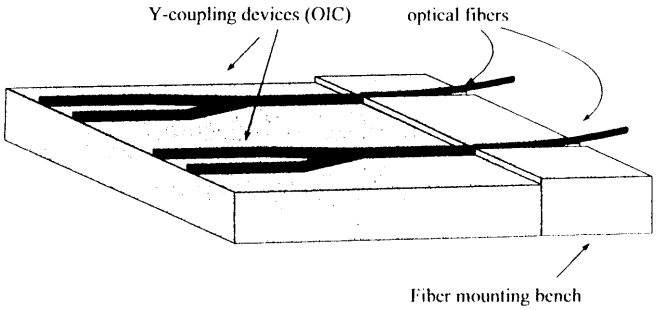

Fig. 1. A coupling concept for fiber-chip coupling using a patterned polymer bench

be adjusted simultaneously by adjusting and fixing the bench, for example on a common substrate. The y_i coordinates are known from the chip production.

1.2 KrF *excimer laser recording*

The excimer laser ablation experiments have been performed at the laser laboratory of the FHO in Emden using a laser of the type EMC-101-MSC (Lambda Physics). A KrF gas filling was used for the experiments at 248 nm. The "beam profile" of the laser was a rectangular area of 8 mm × 28 mm. The maximum pulse energy was 250 mJ per pulse at a frequency of 50 Hz and a half-width duration of 50 ns.

The experimental setup for the laser beam recording is shown in Fig. 2. A slit diaphragm of 1 mm width was homogeneously exposed and focused on the sample using a cylindric lens with a focal length of 10.4 cm. With this cylindric lens the full length of the bench, which is 5 mm in our example, is exposed in its full length. The y_i positions are chosen by the computer-controlled stepping-motor-driven y stage with an accuracy of $\pm 2.54\,\mu$m (10^{-4} inch). The distance between the surface of the sample and the cylindric lens d may be varied in the vicinity of $f = 10.4$ cm.

The minimum half width of the focused laser beam a is given by: [6, 9]

$$a = f\,\lambda/\pi w_0\,, \tag{1}$$

with the focal length f, $\lambda = 248$ nm and $w_0 =$ half width of the unfocused beam. In our case we obtain a theoretical minimum half width of 32 μm in the focal plane.

The maximum pulse energy reaching the sample in the setup is limited due to the geometry to ≈ 5.5 mJ/pulse ($250\,\text{mJ} \times (5 \times 1)/(8 \times 28)$). Assuming a minimum half width of 50 μm at the sample and a length of 5 mm an energy density of $5.5\,\text{mJ}/(50\,\mu\text{m} \times 5\,\text{mm}) = 2.2 \times 10^4\,\text{J/m}^2$ per pulse is obtained and at frequencies between 1 Hz and 50 Hz a power between 0.0056 W and 0.279 W is available at the sample surface, neglecting reflection and scattering losses.

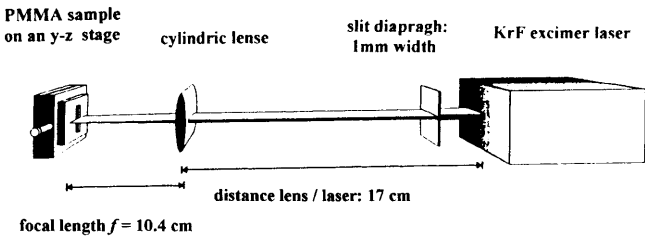

Fig. 2. Arrangement for recording grooves in PMMA samples with an excimer laser

2 Experimental results and discussion

Due to the dimensions of monomode optical fibers the corresponding groove patterns have to be of the order of 100–150 μm in width. Assuming the core diameter of 5–8 μm in the vicinity of the surface, the depth should be about half of the width at minimum, depending on the shape of the groove. Therefore patterns with an aspect ratio (depth/width) $r > 0.5$ will be required.

In contrast to most other etching studies with excimer laser radiation we will not restrict ourselves to parallel light and thin patterns. In our case the already-formed pattern may influence the light distribution and the ongoing etching procedure. Therefore we have to consider different shapes of etched grooves. The dimensions width and depth are related to the actual shape of the groove. Therefore these have to be considered first.

2.1 Characterization of the shape of the recorded grooves

The end faces of the etched PMMA benches have been recorded via microscope as a 2-dimensional pattern and scanned into the computer memory . For comparison a scale is recorded as a reference. A typical result is shown in Fig. 3. The microscope pattern is shown in the left part and the corresponding contrast pattern in the right part of Fig. 3. The determined values for width (221 μm) and depth (375 μm) are indicated as well. As an alternative method for the determination of shape, width, and depth of the recorded grooves a profilometer (Dektak 3030) was used. However the stylus of the profilometer cannot follow the narrow and deep patterns.

The recorded cross sections of the etched grooves can easily be integrated in order to determine the etched volume as a function of the recording parameters.

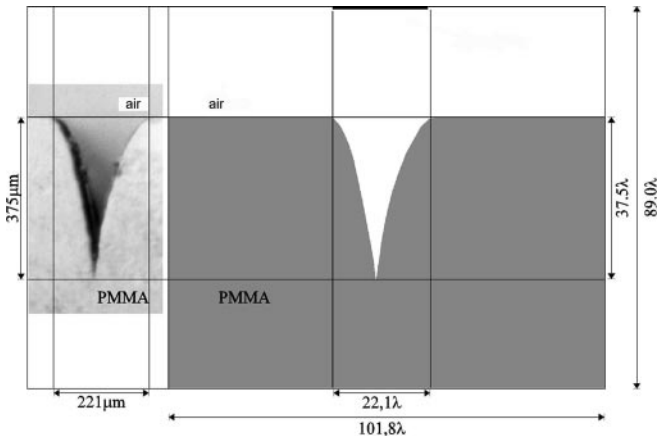

Fig. 3. Typical cross section of a recorded groove; *left*: microscope photograph, *right*: scanned profile

2.2 Shifting the focus point relative to the sample surface

An easy method to change the local intensity distribution of the focused KrF excimer laser light at the surface of the PMMA benches is to change the distance between the sample surface and the cylindric lens. With the change of this distance around the focal length of 10.4 cm patterns of different shape could be obtained. This is shown in Fig. 4 for different distances between lens and sample surface. Viewing the recorded grooves from the top (middle part of Fig. 4) indicates that especially in the middle range of distances smooth thermo-optcal etching is observed without any formation of bubbles or eruptions. However the obtained cross section (top and bottom of Fig. 4) of the groove depends on the distance between sample and lens. From the upper left to the lower right the distance starts at 14.7 cm and is decreased by 0.5 cm per step down to 7.2 cm. The aspect ratio is clearly increased without changing the laser output parameters. In Fig. 5 the parameters depth (full circles) and width of the etched grooves are given for a different distance of lens to sample. Starting at low values with the focal point being beyond the surface of the sample wide and shallow grooves are produced. With the focal point moving towards the surface of the sample the grooves become deeper and narrower. The optimum in the aspect ratio of almost 3:1 is clearly achieved for values of $d \approx 12$ cm with the focal point being well above the surface of the sample. However we have to consider the different shapes of the grooves, shown in Fig. 4. When the distance d passes through the focal length $f = 10.4$ cm, the pattern changes from a "smooth V" to a "sharp V" according to Fig. 4. For $d > 12$ cm there is a clear drop in the depth, the groove becomes flat and shallow again. In addition to this information viewing the grooves from the top shows that in those cases where the focal point is in the material, but significantly below the surface (here at $d \leq 9.2$ cm) a rough surface is obtained due to bubbles and eruptions (Fig. 4, middle, left). Depending on the desired pattern the optimum distance d is in the range between 10 and 12 cm.

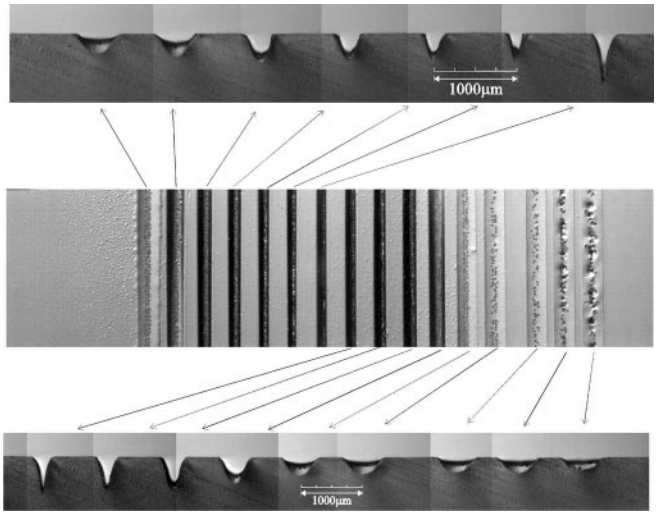

Fig. 4. Variation of the groove pattern with different distance d between the cylindric lens and the sample surface for 14.7 cm (*upper left*) $\geq d \geq$ 7.2 cm (*lower right*) in steps of 0.5 cm

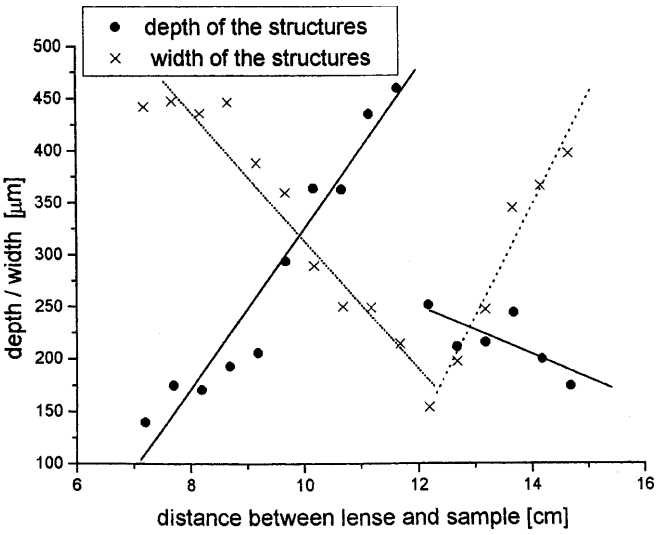

Fig. 5. Depth and width of the obtained grooves as a function of distance d between lens and sample surface (same values as in Fig. 4: 7.2 cm $\leq d \leq$ 14.7 cm)

2.3 Adjusting width and depth of the fiber grooves

With the optimized distance between lens and sample the groove pattern is fixed. Using the full capacity of the computer-controlled adjustment in the y direction an additional shaping of the groove may be obtained by a multi-pulse technique. In this technique a certain number of pulses is applied, while the sample is shifted by a few µm in the y direction. A more detailed investigation has been given in [11], where it has been shown for a multi-pulse technique at 3 positions (0, and $\pm y$) that reproducible and adjustable "V-grooves" may be fabricated with this technique.

In the recording with excimer lasers a convenient parameter is the number of pulses which may easily be controlled and adjusted. In Fig. 6a we have plotted the width and the depth of grooves fabricated at a certain distance $d = 10.2$ cm and a fixed pulse energy. This distance was chosen because the obtained form of the groove pattern was a smooth one according to Fig. 4 without the formation of the sharp "V-form" with some self-focusing effect. The width for these grooves is approaching a saturation value at about 30 laser pulses, while the depths increase linearly with the number of pulses following a constant etching rate of about 1.6 µm per pulse. At about 27–29 pulses there is a step in the measured depth. After that however the slope seems to be the same. If we calculate the etched volume by numerically integrating the shape of the groove and multiplying by the length of the groove, this behavior becomes even more obvious. As can be seen in Fig. 6b above and below the unsteady step we get the same value for the linear regression and we may call it the "etching rate". Therefore we have to assume a change between the subsequent experiments up to 27 pulses and the next one at 28 pulses and onward.

2.4 Using the recorded grooves for coupling

According to the coupling concept illustrated in Fig. 1 the bench containing the monomonde fibers has to be placed in

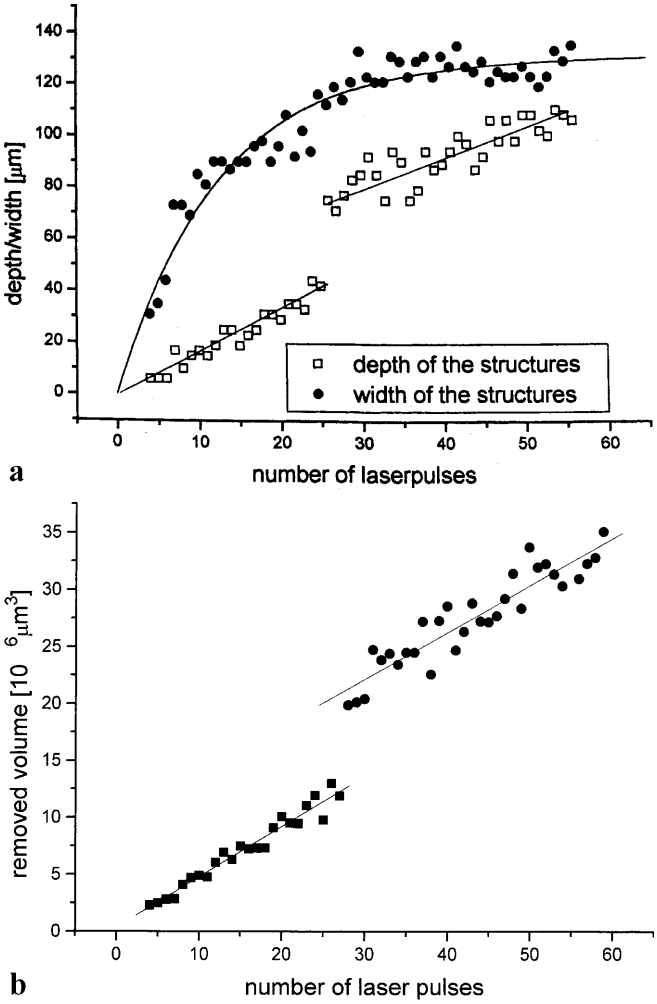

Fig. 6. a Depth and width as a function of laser pulses for a constant distance $d = 10.2$ cm and a constant pulse energy and frequency (250 mJ at 1 Hz), *solid lines* represent a spline function. **b** Etched volume as a function of laser pulses, evaluated data from **a** (*filled squares*: below 27 pulses, *filled circles*: above 28 pulses)

front of the substrate with the waveguide pattern. Both surfaces of the bench and waveguide film have to be at the same level to achieve the best coupling. In Fig. 7 is demonstrated how the relative alignment of the fiber core with the surface or waveguide level can be achieved by choosing the right number of excimer laser pulses for exposure at fixed laser energy and geometrical recording conditions. This result was obtained with a near-field measurement setup. The bright spot indicates the light coming out of the fiber core and the line indicates the surface of the polymer bench, which is supposed to be adjusted to the waveguide on an adjacent substrate according to Fig. 1. The front face of the polymer bench has not been polished. As can be seen from Fig. 7 there is enough room for glue to fix the bottom of the fiber.

3 Simulation

The results obtained in Figs. 4 and 5 indicate that the use of focused excimer laser radiation leads to etched groove patterns with very pronounced narrow front faces, in our case especially in the range of 10 cm $< d <$ 12 cm with $f = 10.4$ cm. This region is especially interesting for etching deep patterns or cutting the material. The obtained results give hints for some self-focusing effects occuring during the interaction of the already-formed pattern with the incoming radiation. In order to investigate this hypothesis we performed the following simulations.

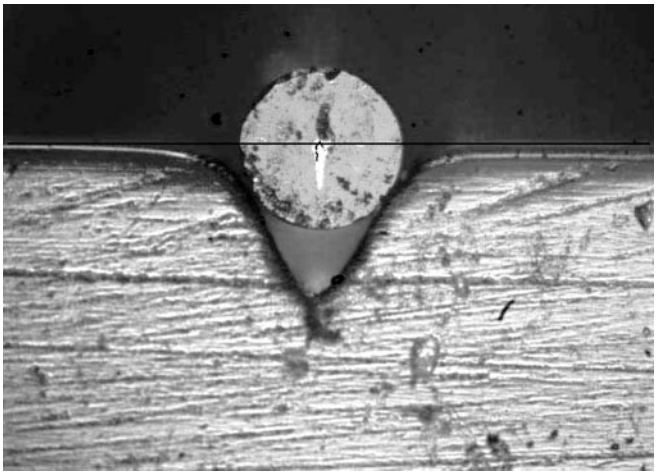

Fig. 7. A typical silica monomode fiber in a recorded groove; The photograph was taken on an optical near-field setup with the bright spot indicating the fiber core

3.1 FDTD simulations of light penetration

The light propagation in integrated optical devices is usually simulated by the widely used beam propagation methods (BPM) [12, 13]. This method is however restricted to the light propagation parallel to one axis. Improved methods are the finite-difference (FD) BPM [14] and the wide-angle BPM [15]. Another approach, which is based on the explicit solution of Maxwell´s equations by means of the finite-difference time-domain (FDTD) method [16, 17] has been implemented on massive parallel computers [18]. For this investigation the same computer system as the one described in [18] has been used.

The propagation of a plane wave entering an ideal V-groove is shown in Fig. 8. The simulation parameters are listed in Table 1. The electric field of the light wave is shown in a grey-tone picture. The higher the contrast between maxima and minima, the higher the amplitude and the intensity. The result of the simulation is in agreement with Snell´s law indicated by the angles of incidence α, the angle of β in the polymer and the angle of reflection α. After entering the material the two beams are basically divergent with an intensity below 50% of the total power. The reflected part of the intensity hits the opposite interface of the V-groove. One part (about 95%) is again transmitted into the material and the reflected part hits the first interface and so on. The darker pixels represent a higher local intensity. At the bottom of the V-groove there is a significant residual intensity which could drive the etching process at this position. Before we look into further details of this intensity we would like to replace the ideal V-pattern by the real V-images, which have been created by focused excimer laser radiation (Fig. 3).

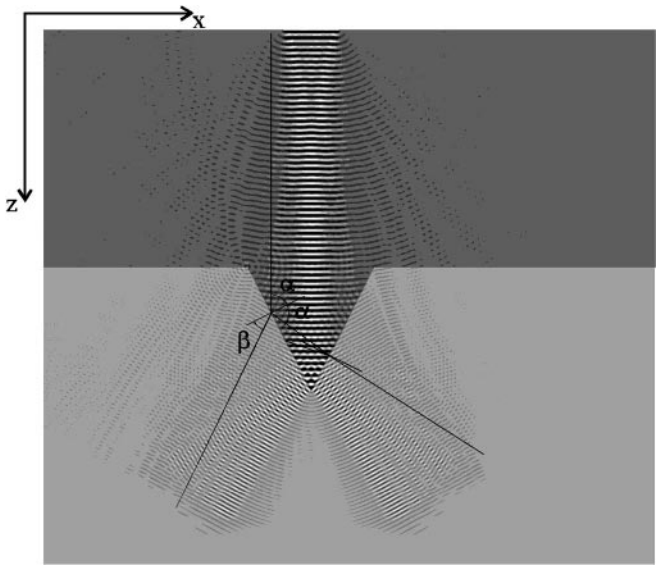

Fig. 8. FDTD simulation of a plane wave entering the area of an ideal V-groove, the simulation parameters are given in Table 1

Table 1. Simulation parameters for the FDTD simulation of light penetration in an idealized "V-groove" (in the *xz* plane) describing the simulation shown in Fig. 8

Parameter	FDTD simulation
polarization	TE
discretization mesh	1018×890
used processors	8×7 slaves, 1processor
discretization cells / processor	128×128
number of iteration steps	3500
vacuum wavelength λ_0	1.00 μm
angle of incidence	parallel to *z* axis
excitation (incoming radiation profile)	90 elements, in the center of the upper simulation edge, (rectangular shape)
refractive index of the medium	1.49 (PMMA), no absorption
refractive index of the environment	1.00
maximum *x* expansion	21.0 μm
maximum *z* expansion	20.5 μm
distance between surface and excitation	39.5 μm

Table 2. Parameters of the FDTD simulation (Fig. 9) of light penetration in a "real, excimer laser patterned V-groove" in the *xz* plane

Parameters	FDTD simulation
polarization	TE
discretization mesh	1018×890
simulated area	$101.8\lambda \times 89.0\lambda$
number of discretization cells/processor	128×128
number of simulated steps	2900
vacuum wavelength λ_0	10 μm
angle of incidence	parallel to *z* axis
excitation (incoming light)	22.1λ in the center of the upper edge of the simulated area (rectangular)
refractive index of the polymer	1.49 (PMMA) no absorption
refractive index of the environment	1.00
maximum size of the *x* expansion	22.1λ
maximum size of the *z* expansion	37.5λ

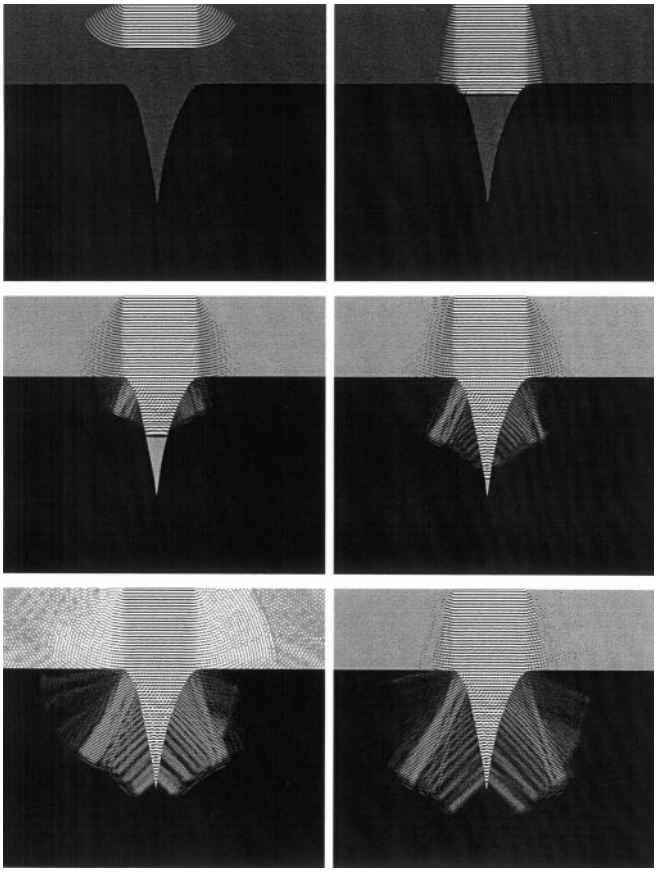

Fig. 9. FDTD simulation of a plane wave entering the area of a real V-groove, for different numbers of simulation steps: from *upper left* to *lower right*, 500, 1000, 1500, 2000, 2500, and 3000 steps; the simulation parameters are given in Table 2

In Fig. 9 the FDTD simulation of a plane wave entering such a real V-groove (as recorded) is shown from the upper left to the lower right as a function of simulation steps. The parameters used for this simulation are listed in Table 2. Basically there is a similar behavior as in case of the ideal V-groove of Fig. 8. Again at the lower tip of the pattern there is a significant contribution to the light intensity. There is a high amplitude in the lowest part of the groove. This high amplitude is obviously responsible for the ongoing etching at the front leading to very sharp grooves.

3.2 FDBPM simulations of pattern formation

The simulation of light interacting with a V-groove requires a 3-dimensional description. The described method implies an effective index method [19], in order to project the 3-dimensional simulation room on the *xz* plane. Furthermore we make the following assumptions for the following model of pattern formation:

- a parallel laser with a Gaussian intensity profile hits perpendicularly the surface of the polymer PMMA
- when the laser beam hits the surface, material is removed according to the following assumptions:
  a) Material is only removed from the surface. Evaporation or photochemical reactions are neglected.

b) Previous damage of the bulk material during the period of one single pulse is not considered.
c) Between any subsequent laser pulses the sample cools down to the initial value.
d) Material decomposes when it is heated to its decomposition temperature by absorbing a critical amount of light.
e) Absorption is 100% in the upper discrete layer of the material. The absorption in the bulk material is neglected.

This model is illustrated in Fig. 10. The Gaussian lineshape causes, according to the assumptions above, a partial etching of those volume cells where the absorbed intensity was above the critical level. The next light pulse (Fig. 10c) hits a modified surface, the refractive index of the etched cells has been switched from 1.49 to 1.00 and so on. In Fig. 11 the simulated interaction of a Gaussian-shape laser beam with the forming surface pattern is shown as a sequence from the upper left to the lower right. After two iterations (upper left) the beam is still undisturbed, because the surface is still flat. After 10 iterations a slight distortion becomes obvious. The "V" pattern appears after 50 iteration cycles. Starting with 70 cycles the splitting of the beam can be observed. After 240 iterations (lower right) the intensity is no longer penetrating parallel to the z axis in the material below the etched pattern. This is comparable to the results in Sect. 3.2 for an ideal (Fig. 8) and a real etched "V-groove" (Fig. 9). However at the lowest point of the groove there seems to be some focusing effect.

From this simulation we have calculated the local intensity distribution. The result is shown in Fig. 12. In the free space there is the Gaussian intensity distribution entering the graph at the $z = 0$ plane. The position of the lowest point of the "V-groove" ($y = 0$) refers to the point when the smooth intensity pattern is changing. The most striking result of this simulation is the observation that in the lower tip of the groove on the $y = 0$ plane the intensity is piling up, reaching higher values than the maximum intensity in the unperturbed beam (in Fig. 12: 200 vs. 110). In terms of etching this region should be the one with preferred etching. The intensity distribution shown in Fig. 12 would give rise to an etching process similar to the one observed in the experimental part in Figs. 4 and 5 with $10\,\text{cm} < d < 12\,\text{cm}$.

With the above assumptions we obtain etched grooves like the one shown in Fig. 13. This is very similar to the experimental results shown in Fig. 4 for focused excimer laser radiation in the range of $10\,\text{cm} < d < 12\,\text{cm}$ with a focal length $f = 10.4\,\text{cm}$. Although a qualitative agreement could be achieved the theoretical model is still different from the experimental circumstances.

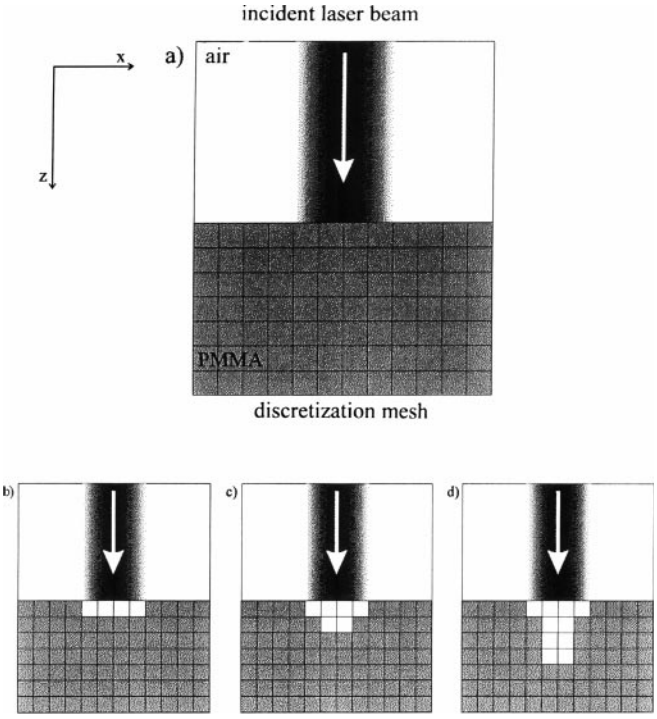

Fig. 10. Scheme of the assumed model for the simulation of groove formation during excimer laser beam etching

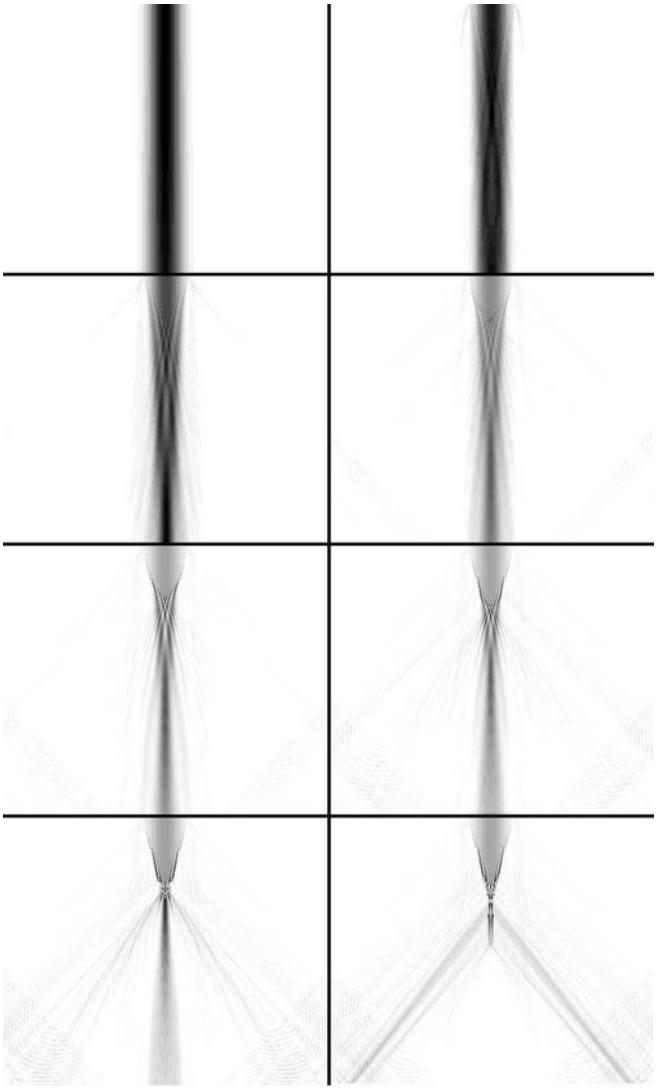

Fig. 11. FDBPM simulation of the laser intensity during the etching process according to the model described in Fig. 10 after different simulation steps from *upper left* to *lower right*: 2, (Gaussian), 10 (surface already modified), 120, and 240

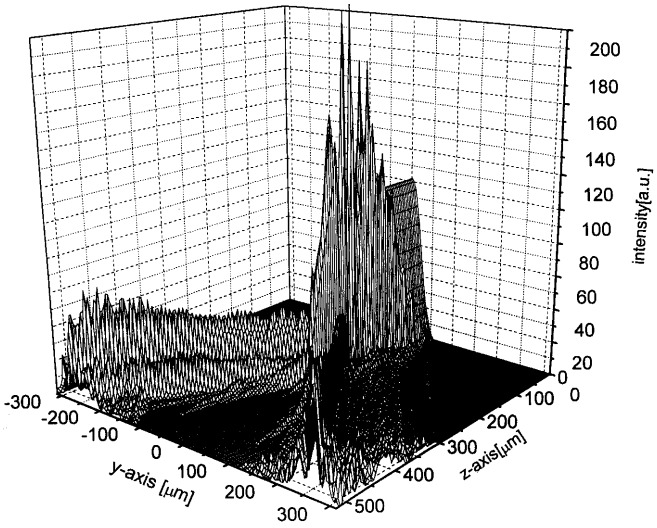

Fig. 12. Resulting light intensity pattern after 240 cycles. For demonstration purposes the pattern has been rotated by 90°

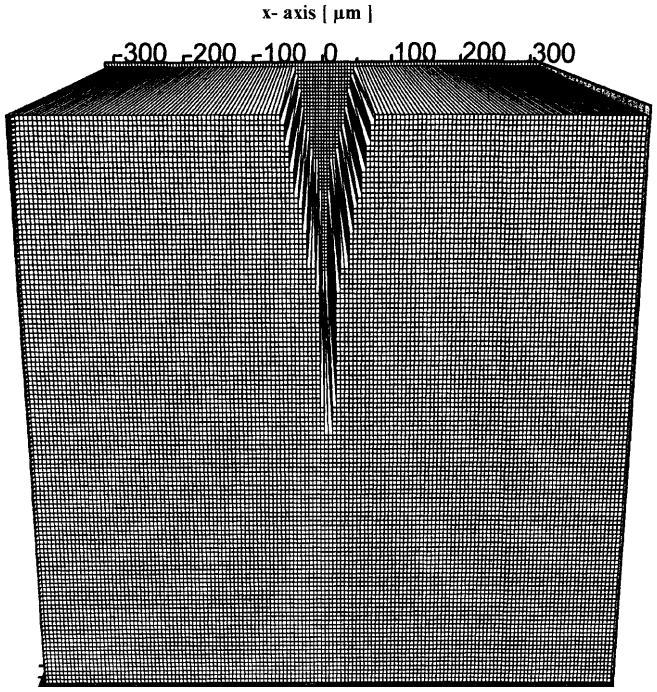

Fig. 13. Simulated pattern recorded according to the model discussed in Sect. 3.2 width = 86 µm, depth = 219 µm after 240 simulation steps (saturation)

4 Conclusions

The process of deep etching with focused excimer laser radiation has been studied for the example of one particular application, the formation of grooves for the optical monomode fiber using cylindric lenss. The form of the grooves could be adopted in a wide range between a "V" and a "U" form by specially optimized multipulse computer-controlled techniques.

By choosing a particular form of groove its width and its depth could be controlled by the number of laser pulses.

The technique of deep etching with focused excimer laser radiation has been simulated by two different approaches. The first one uses the FDTD method and explains the interaction of a plane Gaussian wave with the intermediate grooves. The local distribution of intensity explains the observed etching process. The second method uses a simple model for thermo-optic etching and the FDBPM approach using a planar Gaussian beam suggests a form of etched groove that is very similar to the ones obtained in the experimental part.

Acknowledgements. T. Sterkenburgh and H. Franke wish to thank the DFG (Fr 855/1) and Deutsche Telekom for financial support.

References

1. R. Srinivasan, V. Mayne-Banton: Appl. Phys. Lett. **41**, 576 (1982)
2. H. Pummer: Phys. Blätter **41**, 195 (1985)
3. P.G. Berrie, F.N. Birkett: Optics and Lasers in Engineering **1**, 107 (1980)
4. R. Joecklé: Proc. of the Int. Conf. on Lasers, p. 1025 (1989)
5. A. Donat, K. Deiters: Feingerätetechnik **33**, 307 (1984)
6. S.S. Charschan (Ed.): *Lasers in Industry* (Von Nostrald-Reinhold, New York 1987)
7. C. Dinger, T. Sterkenburgh, T. Holler, H. Franke: SPIE Proc. **1774**, 278 (1992)
8. T. Sterkenburgh, S. Nischwitz, H. Franke: Photonics West, San Jose, SPIE Proc. **2686**, 37 (1996)
9. S.S. Charschan (Ed.): *Lasers in Industry* (Von Nostrald-Reinhold, New York 1972)
10. L. Dorn, F. Herbert, S. Jafari, D. Purst: Laser und Optoelectronik **4**, 37 (1995)
11. T. Sterkenburgh, H. Franke, M.G. Becker, W. Garen, W.F.X. Frank: SPIE Proc. **3135**, 134 (1997)
12. J.A. Fleck, J.R. Morris, M.D. Feit: Appl. Phys. **10**, 129 (1976)
13. S.M. Saad: IEEE Trans. Microwave Theory Tech. **MTT-33**, 894 (1985)
14. D. Yevick, B. Hermansson: IEEE J. Quantum Electron. **QE-26**, 109 (1990)
15. G.R. Hadley: Opt. Lett. **17**, 1426 (1992)
16. K.S. Yee: IEEE Trans. Antennas Propag. **AP-14**, 302 (1966)
17. A. Wexler: IEEE Trans. Microwave Theory Tech. **MTT-17**, 416 (1969)
18. T. Sterkenburgh, R.M. Michels, H. Franke: Appl. Opt. **36**, 1191 (1997)
19. T. Tamir: *Guided Wave Optoelectronics* (Springer, Berlin, Heidelberg 1990)